LBL-34513
UC-414
Preprint

Lawrence Berkeley Laboratory

UNIVERSITY OF CALIFORNIA

Accelerator & Fusion Research Division

Submitted to Fifth Special Issue on High Power Microwaves
of the IEEE Transactions on Plasma Science

Three-Dimensional Simulation Analysis of a 3-cm Wavelength Free-Electron Laser Afterburner

C. Wang

August 1993

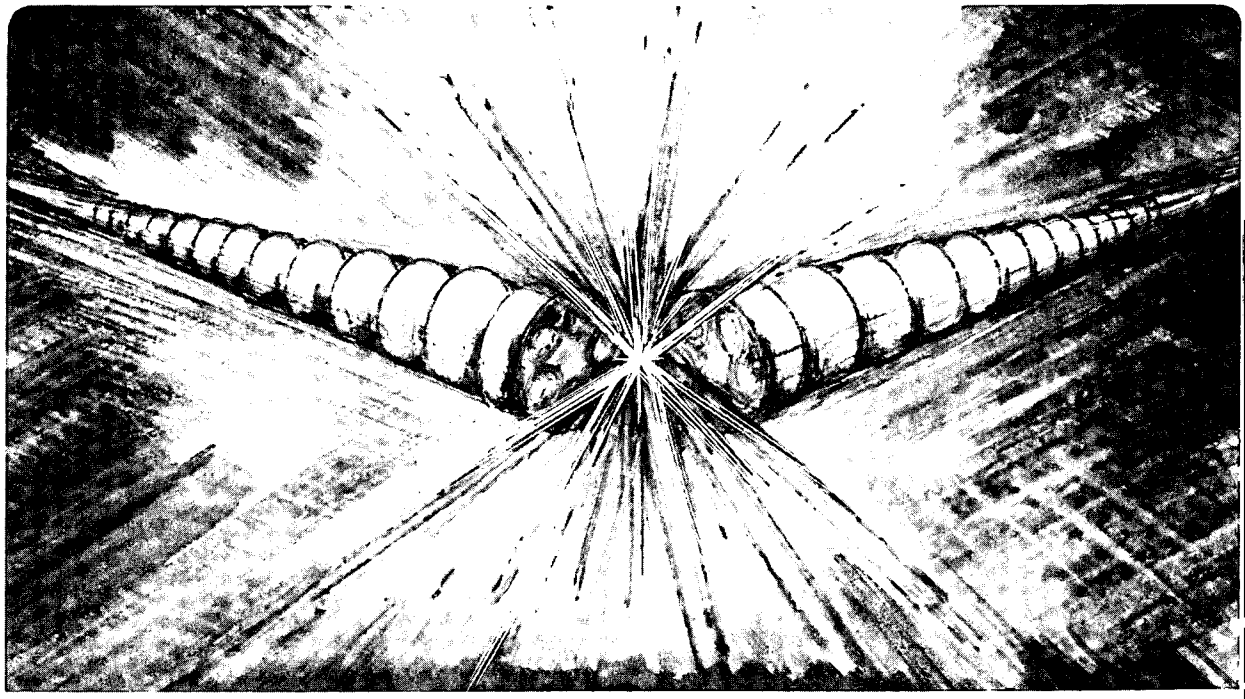

REFERENCE COPY
Does Not
Circulate
Bldg. 50 Library.
LBL-34513
Copy 1

Prepared for the U.S. Department of Energy under Contract Number DE-AC03-76SF00098

DISCLAIMER

This document was prepared as an account of work sponsored by the United States Government. While this document is believed to contain correct information, neither the United States Government nor any agency thereof, nor the Regents of the University of California, nor any of their employees, makes any warranty, express or implied, or assumes any legal responsibility for the accuracy, completeness, or usefulness of any information, apparatus, product, or process disclosed, or represents that its use would not infringe privately owned rights. Reference herein to any specific commercial product, process, or service by its trade name, trademark, manufacturer, or otherwise, does not necessarily constitute or imply its endorsement, recommendation, or favoring by the United States Government or any agency thereof, or the Regents of the University of California. The views and opinions of authors expressed herein do not necessarily state or reflect those of the United States Government or any agency thereof or the Regents of the University of California.

LBL-34513
CBP-034
UC-414

Three-Dimensional Simulation Analysis of a 3-cm Wavelength Free-Electron Laser Afterburner*

Changbiao Wang

Lawrence Berkeley Laboratory, University of California, Berkeley, California 94720

August 1993

* Work supported by the Director, Office of Energy Research, Office of High Energy and Nuclear Physics, Division of High Energy Physics, of the U.S. Department of Energy under Contract No. DE-AC03-76SF00098

Three-Dimensional Simulation Analysis of a 3-cm Wavelength Free-Electron Laser Afterburner

Changbiao Wang[a]

Center for Beam Physics, Lawrence Berkeley Laboratory
University of California, Berkeley, California 94720

Abstract---We have simulated a 3-cm wavelength free-electron laser afterburner (FEL Afterburner) using two sets of parameters: one is for a 3-cm period wiggler and the other is for a 5.4-cm period wiggler. For the 3-cm period wiggler, the input beam energy is 112.5 keV, and for the 5.4-cm period wiggler the beam energy is increased to 290 keV to make the FEL Afterburner operate at the same frequency. It is found, from the simulations, that the FEL Afterburner with a longer period wiggler has a higher power conversion efficiency: larger than 16% for the 5.4-cm wiggler while only about 9% for the 3-cm wiggler. It is also shown that to enhance the interaction efficiency in the slow wave cavity, the slow wave number should be a little larger than the sum of the fast wave number and the wiggler wave number.

[a] Permanent address: High Energy Electronics Research Institute, University of Electronic Science and Technology of China, Chengdu, Sichuan 610054, China.

I. Introduction

The free-electron laser afterburner is a new kind of microwave power device, which consists of a FEL buncher and a slow wave structure. The FEL buncher makes an electron beam bunched in the longitudinal direction while high power microwaves are generated in the slow wave structure by the interaction of the beam with the longitudinal component of the slow wave electric field. A FEL Afterburner with a 20-cm period wiggler was investigated and it was shown that an efficiency of up to 28% could be obtained, at 17.12 GHz, from a 1-kA, 5-MeV electron beam [1]. In that FEL Afterburner the wiggler period was quite long compared with the operating wavelength and so the device was relatively long. If a low energy beam (a few hundred keV, for example) is used, the wiggler period can be greatly shortened and the FEL Afterburner will be much more compact.

In this paper, we present three-dimensional simulation results for a 3-cm wavelength FEL Afterburner with an electron beam energy of the order of a few hundred keV. The 3-cm wavelength FEL Afterburner, as shown in Fig.1, has three cavities, and it is simulated using two sets of parameters. In the three cavities, two are fast wave cavities and one is a slow wave cavity operating in the standing-wave state. It is assumed that only a simplified form of longitudinal slow wave field exists in the slow wave cavity [1]. The main difference between the first and the second sets of parameters is that the wiggler period is different, one being 3 cm and the other being 5.4 cm, and each with its corresponding appropriate beam energy. For the 3-cm period wiggler, the input beam energy is only 112.5 keV, and for the 5.4-cm period wiggler, the beam energy is increased to 290 keV to make the FEL Afterburner operate at the same frequency. It is found from the simulations that the FEL Afterburner with a longer period wiggler has a higher power conversion efficiency: larger than 16% for the 5.4-cm wiggler while only about 9% for the 3-cm wiggler. It is also found that to enhance the interaction efficiency in the slow wave cavity, the slow wave number should be a little larger than the sum of the fast wave number and the wiggler wave number.

II. Simulation Parameters

The wiggler used in the simulation is the combination of a helical wiggler and a uniform guided magnetic field and they are given by

$$B_x = T(z)B_{w0}\left[I_0(k_w r)\cos(k_w z) + I_2(k_w r)\cos(k_w z - 2\theta)\right] \quad (1)$$

$$B_y = T(z)B_{w0}\left[I_0(k_w r)\sin(k_w z) - I_2(k_w r)\sin(k_w z - 2\theta)\right] \quad (2)$$

$$B_z = -2T(z)\, B_{w0} I_1(k_w r)\sin(k_w z - \theta) + B_0 \quad (3)$$

where B_{w0} is the wiggler amplitude on the axis, B_0 is the axial uniform magnetic field, the wiggler wave number is given by $k_w=2\pi/\lambda_w$ with λ_w the wiggler period, and the tapering factor is given by $T(z)=z/7\lambda_w$ when $z\leq 7\lambda_w$ and $T(z)=1$ when $z>7\lambda_w$.

Here we use seven tapered wiggler periods to make the electrons move in helical orbits. Although the wiggler is helical, the fast wave cavities are rectangular and they operate on the $TE_{1,0,24}$ mode. The slow wave cavity is cylindrical. The two sets of simulation parameters, in which one is for the 3-cm period wiggler and the other is for the 5.4-cm period wiggler, are given in table 1 and table 2, respectively.

III. Simulation Results

In the simulation, an electron beam with no initial energy spread and zero emittance is employed. The input beam energy and current pulse is 40 ns long, including a 2-ns rise time, 36-ns flat top, and 2-ns fall time. For the two sets of parameters, the simulation results follow.

1. First set of parameters (3-cm period wiggler)

Figure 2 shows the longitudinal rf current amplitude and the rms-normalized longitudinal velocity spread versus axial distance for the 35th bucket of the beam. The first cavity is located from 0.21 m to 0.686 m, the second one from 0.72 m to 1.196 m, and the third one from 1.23 m to 1.657 m. The velocity spread reaches its maximum, 1.3%,

almost when the rf current reaches its maximum, 4.9 A, within the slow wave cavity. The averaged current over the slow wave cavity is 3.9 A.

Figures 3 and 4 show the rf output power of the second and the third cavities respectively. The power from the second cavity is about 400 W and is very small, only about 1.4% of that from the third cavity, of which the output power on the flat part is 29.2 kW, corresponding to an efficiency of 8.7%. So the averaged longitudinal velocity of the beam is little changed by the interaction in the second cavity. In such a situation, the slow wave number of the third cavity is almost the same as the sum of the fast wave number and the wiggler wave number.

2. Second set of parameters (5.4-cm period wiggler)

Figure 5 shows the longitudinal rf current amplitude and the rms-normalized longitudinal velocity spread versus axial distance for the 35th bucket of the beam. The first cavity is located from 0.378 m to 0.854 m, the second one from 0.918 m to 1.394 m, and the third one from 1.458 m to 1.902 m. The maximum rf current is 4.7 A and the maximum velocity spread is 2.1%. In contrast to the above case, these maxima are located at different positions within the slow wave cavity. The averaged current over the slow wave cavity is 4.1 A, a little larger than in the first case because the current has a wider peak.

Figures 6 and 7 show the rf output power of the second and the third cavities respectively. The power from the second cavity is 16.9 kW for the flat part, more than 10% of that from the third cavity, of which the output power on the stable part is above 141 kW, and the efficiency is greater than 16.2%. So the averaged longitudinal velocity of the beam is a little decreased by the interaction in the second cavity. The slow wave number of the third cavity is equal to 103% of the sum of the fast wave number and the wiggler wave number, a little larger than the sum.

In free space, the dependence of the rf current of a bunched beam on the axial distance z, along which the beam is moving, can be described by

$$I(z)=I(z_0)\left|\frac{\sin\xi(z-z_0)}{\xi(z-z_0)}\right| \tag{4}$$

where z_0 the initial longitudinal coordinate of the bunched beam, and the debunching parameter $\xi=2\sqrt{3}\pi(\Delta\beta_z)_{rms}\lambda^{-1}\langle\beta_z\rangle^{-2}$ with $(\Delta\beta_z)_{rms}$ the rms-spread in longitudinal normalized velocities, $\langle\beta_z\rangle$ the averaged longitudinal normalized velocity, and λ the free-space wavelength of the drive wave of the bunched beam. When a beam interacts coherently with an rf field, the interaction causes the beam to bunch. However, the spread in longitudinal velocities is increased at the same time and the debunching parameter becomes larger so that the beam has a tendency to be debunched. Before the rf current reaches its maximum the bunching effect is dominant, and after that, the debunching effect is dominatnt. From Figs. 2 and 5, we see that the rf currents reach their maxima within the slow wave cavities, and rapidly decrease with the axial distance which is due to the debunching effect. Figure 8 shows the comparison between the debunching effects in the slow wave cavity and in free space, respectively, for the 3-cm and the 5.4-cm period wigglers. From it we see that the decrease of rf current indeed results from the debunching effect although it is not so fast as in free space because the cavity field has an effect of constraining phase [2].

It should be noted that the debunching parameter is directly proportional to the rms-velocity spread and inversely proportional to the square of the averaged longitudinal velocity. So the beam with a larger velocity spread may have a smaller debunching parameter if its energy is higher. From Fig. 9, we can see that the debunching parameter for the 5.4-cm period wiggler is smaller than that for the 3-cm period wiggler within the slow wave cavity because the beam has a higher averaged longitudinal velocity. At the current maximum, the debunching parameter takes a value of 15.2 m^{-1} for the 3-cm case

while only 11.2 m^{-1} for the 5.4-cm case. So the rf current has a wider peak for the 5.4-cm case.

Making a proper choice of the external quality factors, which are related to the operating parameters, is very important. Too large quality values may degrade the shape of the output power pulse and too small quality values, however, will result in a very low output power level.

Making a proper choice of input rf power is also very important. The input power should be adjusted so that the rf current reaches its maximum within the slow wave cavity so that maximum output power can be obtained. Too small input power results in a small output power even though the rf current maximum appears within the slow wave cavity. However, too large input power will cause the rf current to reach its maximum before the slow wave cavity so that the output power will be greatly reduced.

IV. Conclusions

We have simulated a 3-cm wavelength FEL Afterburner with a 3-cm period wiggler and a 5.4-cm period wiggler respectively. From the simulations we find that the FEL Afterburner with a longer period wiggler has a higher power conversion efficiency. To keep the beam sychronous with the slow wave in the slow wave cavity and enhance the interaction efficiency, the slow wave number should be a little larger than the sum of the fast wave number and the wiggler wave number.

Acknowledgment

The author would like to thank Andrew M. Sessler for his critical comments and many good suggestions. He also would like to thank Manoel Conde for his helpful discussions. The work was supported by the Director, Office of Energy Research, Office of High Energy and Nuclear Physics, Division of High Energy Physics, of the U. S. Department of Energy under Contract No. DE-AC03-76SF00098.

References

[1] C. Wang and A. M. Sessler, "An Efficient Microwave Power Source: Free-Electron Laser Afterburner," accepted for publication in Journal of Applied Physics.

[2] C. Wang and A. M. Sessler, "Three-Dimensional Simulation Analysis of the First Sections of a Standing-Wave Free-Electron Laser Two-Beam Accelerator", to be published in the proceedings of 1993 Particle Accelerator Conference.

Biography

Changbiao Wang graduated with the Ph. D. degree in electrophysics from University of Electronic Science and Technology of China, Chengdu, China, in 1987, and worked there as a postdoctoral researcher for two years. From August 1991 to now, he has been working as a visiting researcher in the Center for Beam Physics at Lawrence Berkeley Laboratory. He has been engaged in microwave electronics, relativistic electron beam physics, and most recently, two-beam accelerator studies.

Table 1

First set of parameters in the simulation (3-cm period wiggler)

Wiggler period	3 cm
Wiggler amplitude on axis	0.07 T
Axial magnetic field	0.8 T
Beam energy	112.5 keV
Beam current	3 A
Beam radius	2 mm
Fast wave cavity dimension (width×height×length)	2.29 cm×1.02 cm×47.65 cm
Slow wave cavity dimension (radius×length)	1.4 cm×42.72 cm
Wiggler wave number	2.09 (cm^{-1})
Fast wave number	1.58 (cm^{-1})
Slow wave number	3.68 (cm^{-1})
External quality factor	
Cavity 1	30
Cavity 2	30
Cavity 3	10
Drift pipe dimension (radius×length)	
Pipe 1	4 mm×21 cm
Pipe 2	4 mm×3.35 cm
Pipe 2	4 mm×3.35 cm
Input rf power	500 W
Drive frequency	9.8 GHz

Table 2

Second set of parameters in the simulation (5.4-cm period wiggler)

Wiggler period	5.4 cm
Wiggler amplitude on axis	0.08 T
Axial magnetic field	0.8 T
Beam energy	290 keV
Beam current	3 A
Beam radius	2 mm
Fast wave cavity dimension (width×height×length)	2.29 cm×1.02 cm×47.65 cm
Slow wave cavity dimension (radius×length)	1.2 cm×44.4 cm
Wiggler wave number	1.16 (cm^{-1})
Fast wave number	1.58 (cm^{-1})
Slow wave number	2.83 (cm^{-1})
External quality factor	
Cavity 1	350
Cavity 2	300
Cavity 3	25
Drift pipe dimension (radius×length)	
Pipe 1	4 mm×37.8 cm
Pipe 2	4 mm×6.35 cm
Pipe 2	4 mm×6.35 cm
Input rf power	1400 W
Drive frequency	10.01GHz

Figure Captions

Fig. 1. The three-cavity free-electron laser afterburner.

Fig. 2. Longitudinal rf current amplitude and rms-normalized velocity spread versus axial distance for the 3-cm period wiggler.

Fig. 3. Second cavity rf output power versus time for the 3-cm period wiggler.

Fig. 4. Third cavity output power versus time for the 3-cm period wiggler.

Fig. 5. Longitudinal rf current amplitude rms-normalized velocity spread versus axial distance for the 5.4-cm period wiggler.

Fig. 6. Second cavity rf output power versus time for the 5.4-cm period wiggler.

Fig. 7. Third cavity rf output power versus time for the 5.4-cm period wiggler.

Fig. 8. Comparison between the debunching effects in the slow wave cavity (solid curve) and free space (dashed curve) for the 3-cm and the 5.4-cm period wigglers.

Fig. 9. Debunching parameters for the 3-cm and 5.4-cm period wigglers versus axial distance.

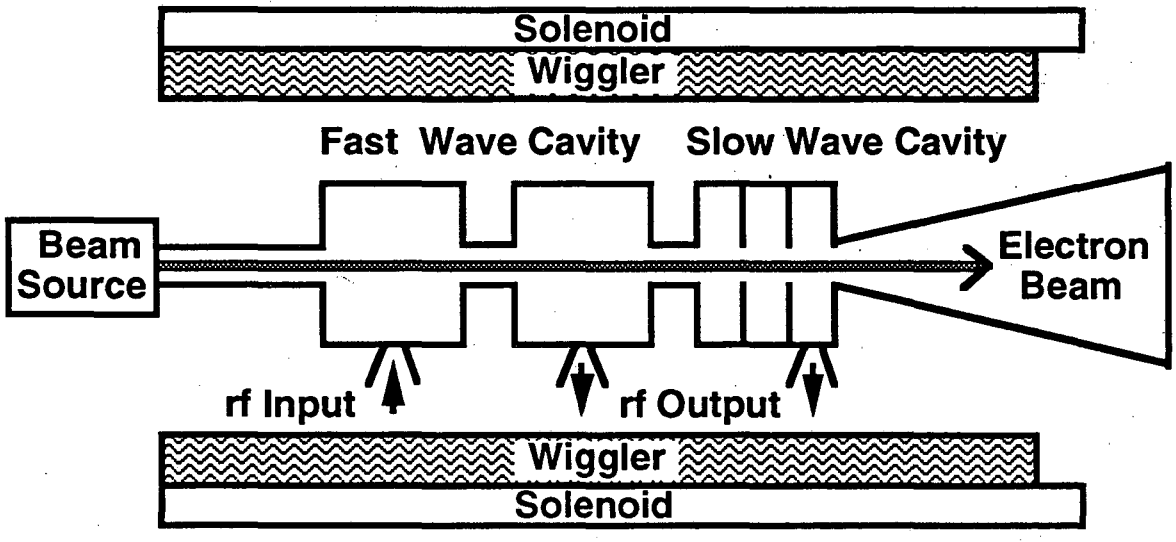
Solenoid
Wiggler
Fast Wave Cavity
Slow Wave Cavity
Beam Source
Electron Beam
rf Input
rf Output
Wiggler
Solenoid

Fig. 1

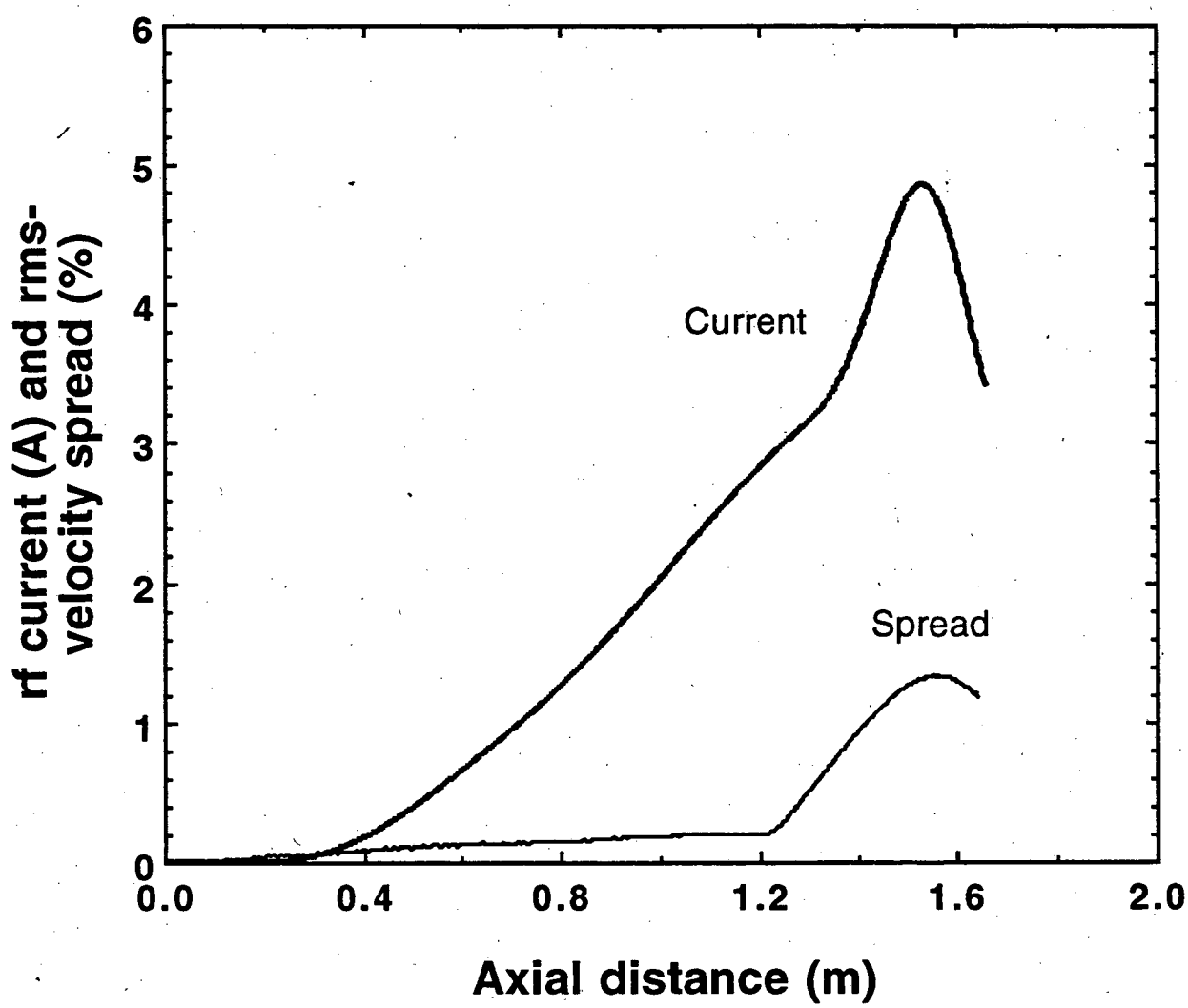
rf current (A) and rms-velocity spread (%)
Axial distance (m)
Current
Spread
0
1
2
3
4
5
6
0.0
0.4
0.8
1.2
1.6
2.0

Fig. 2

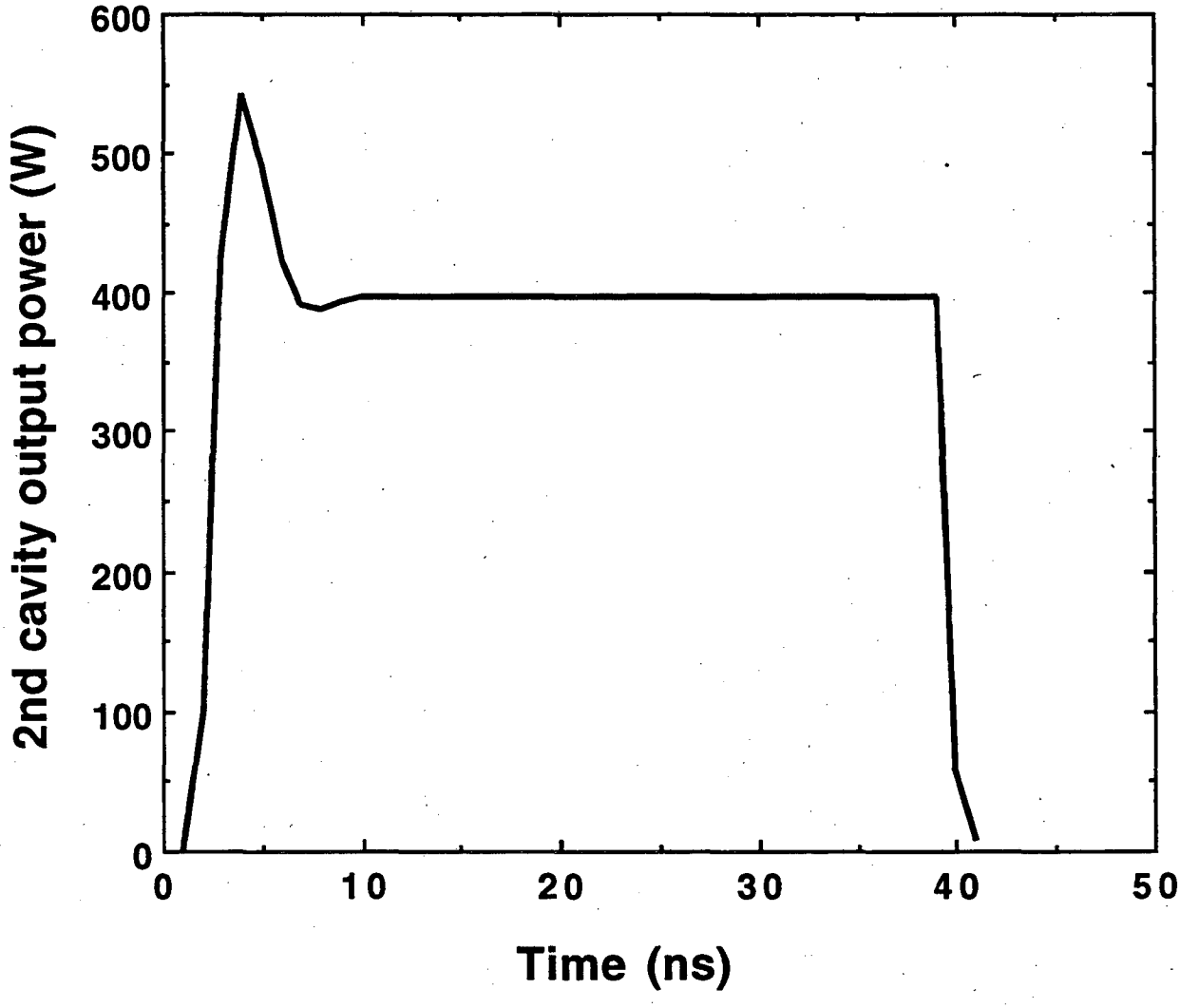
600
500
400
300
200
100
0
2nd cavity output power (W)
0
10
20
30
40
50
Time (ns)

Fig. 3

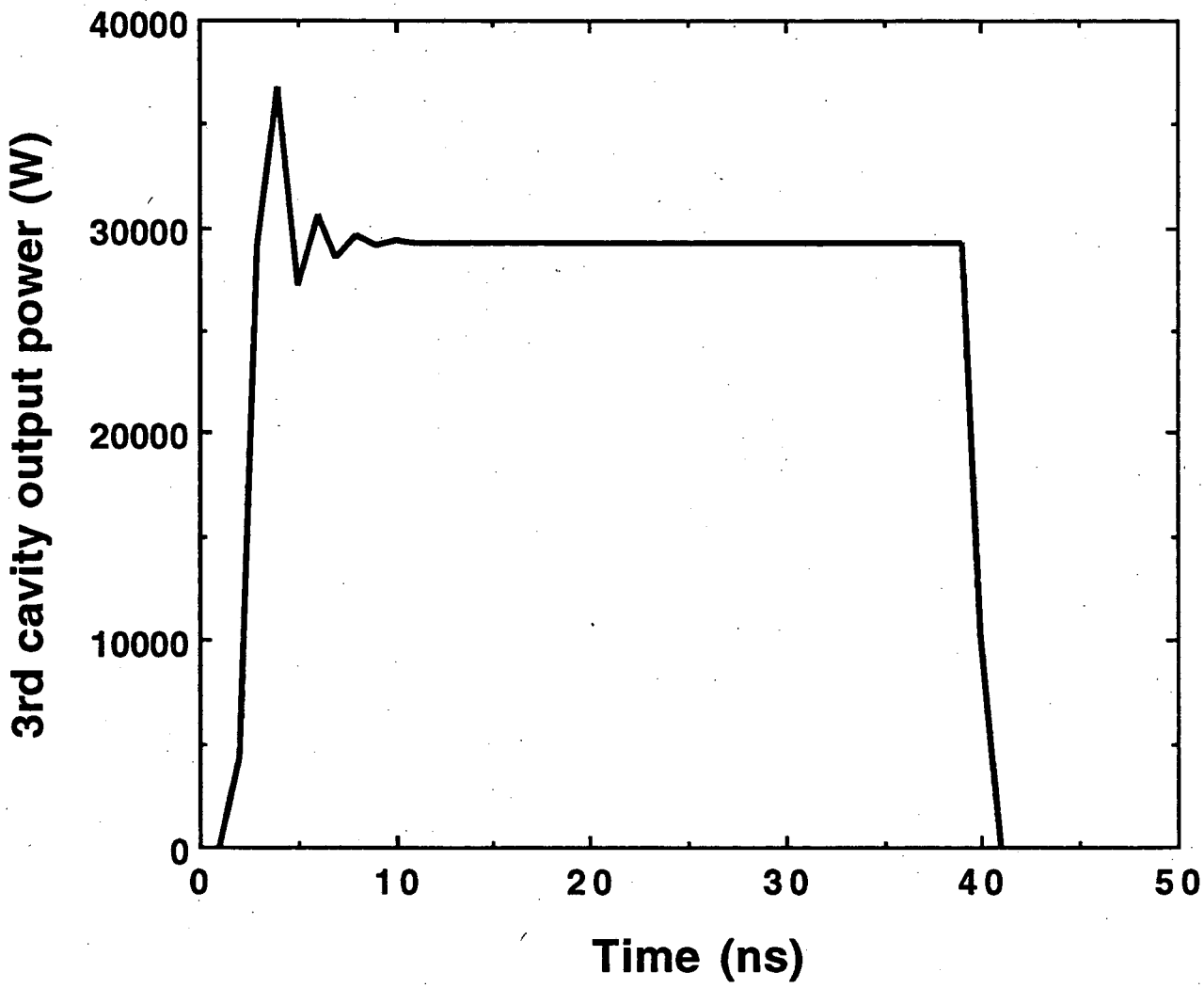
40000
30000
20000
10000
0
3rd cavity output power (W)
0
10
20
30
40
50
Time (ns)

Fig. 4

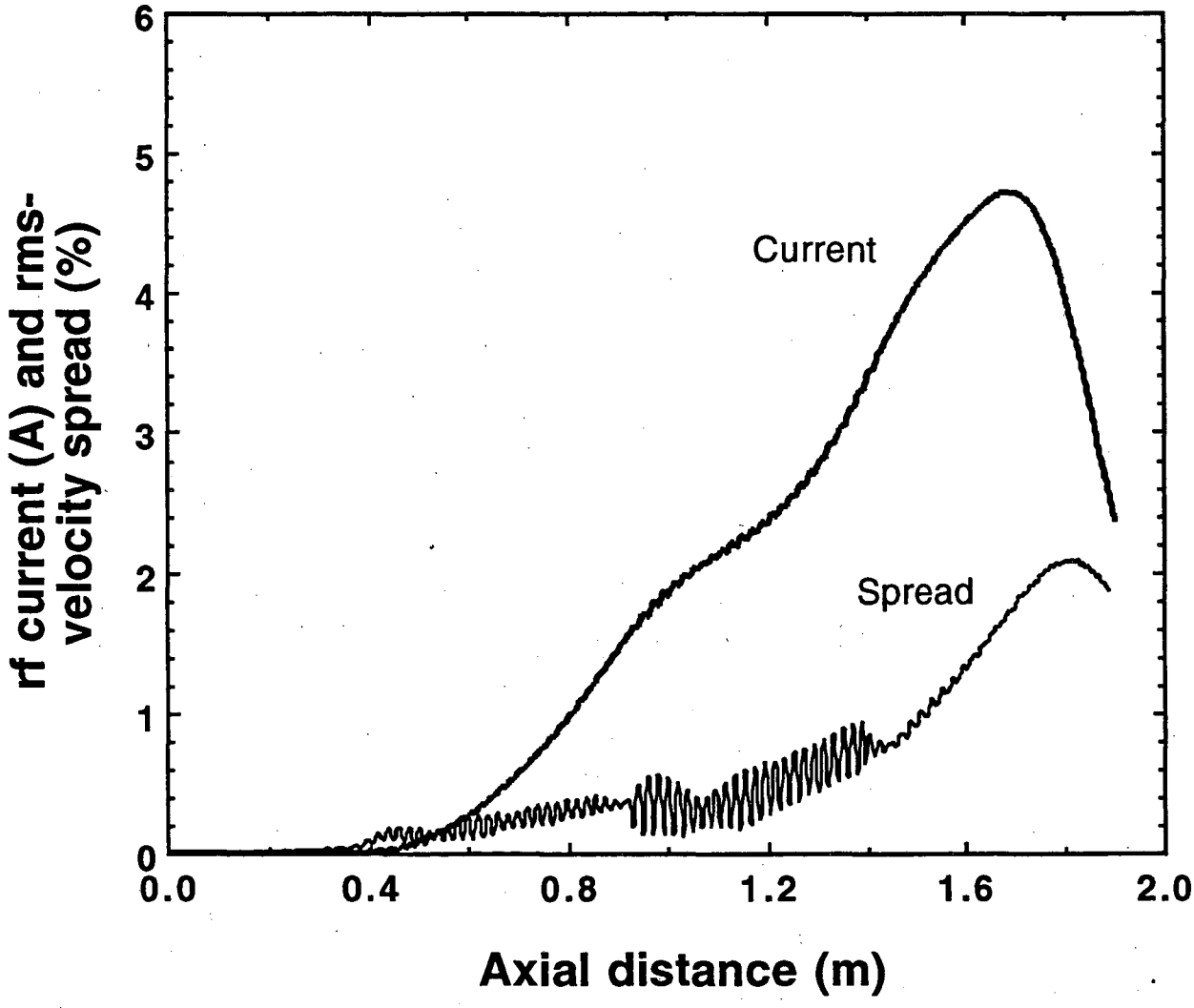
rf current (A) and rms-velocity spread (%)
Current
Spread
Axial distance (m)
0
1
2
3
4
5
6
0.0
0.4
0.8
1.2
1.6
2.0

Fig.5

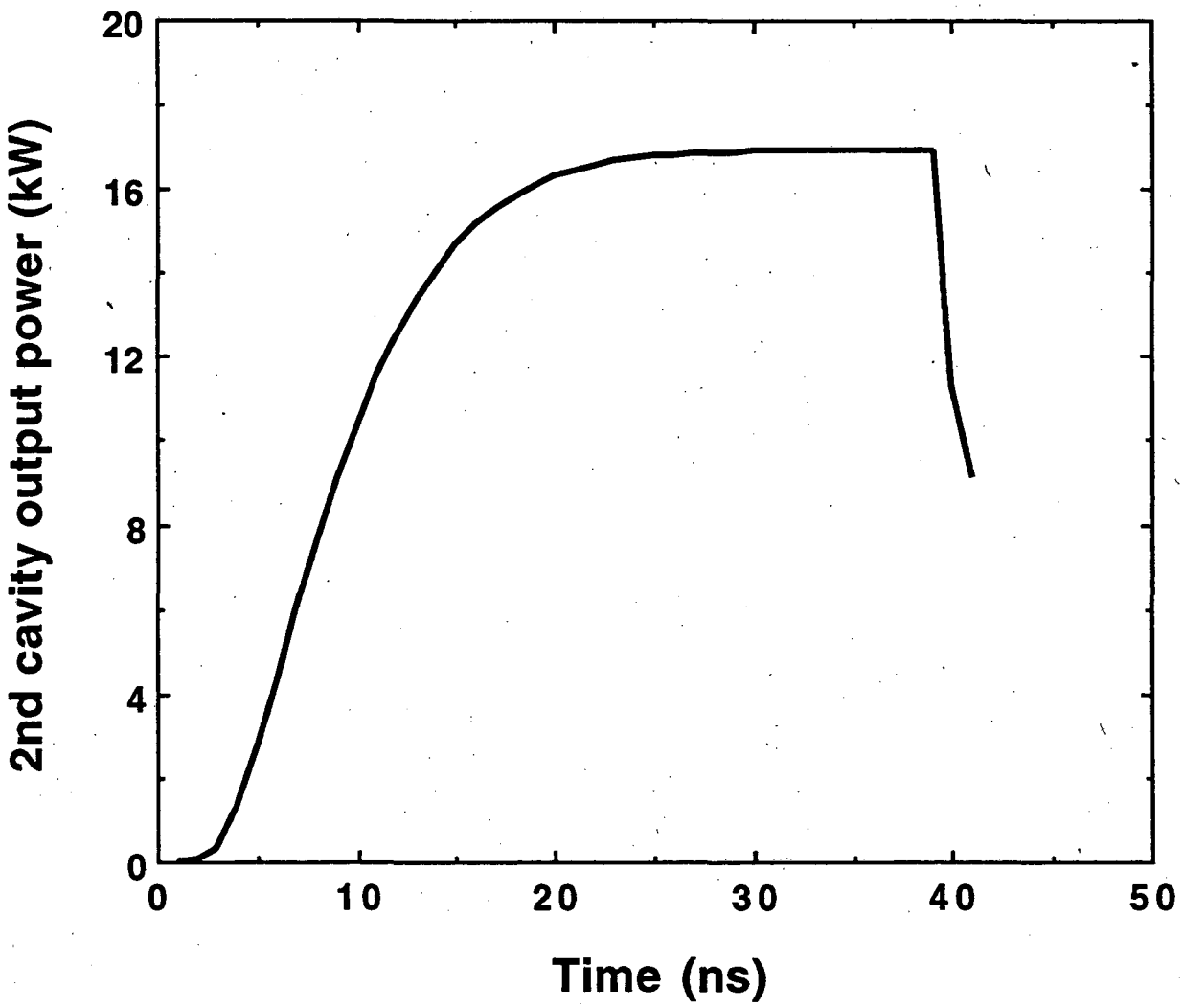

Fig.6

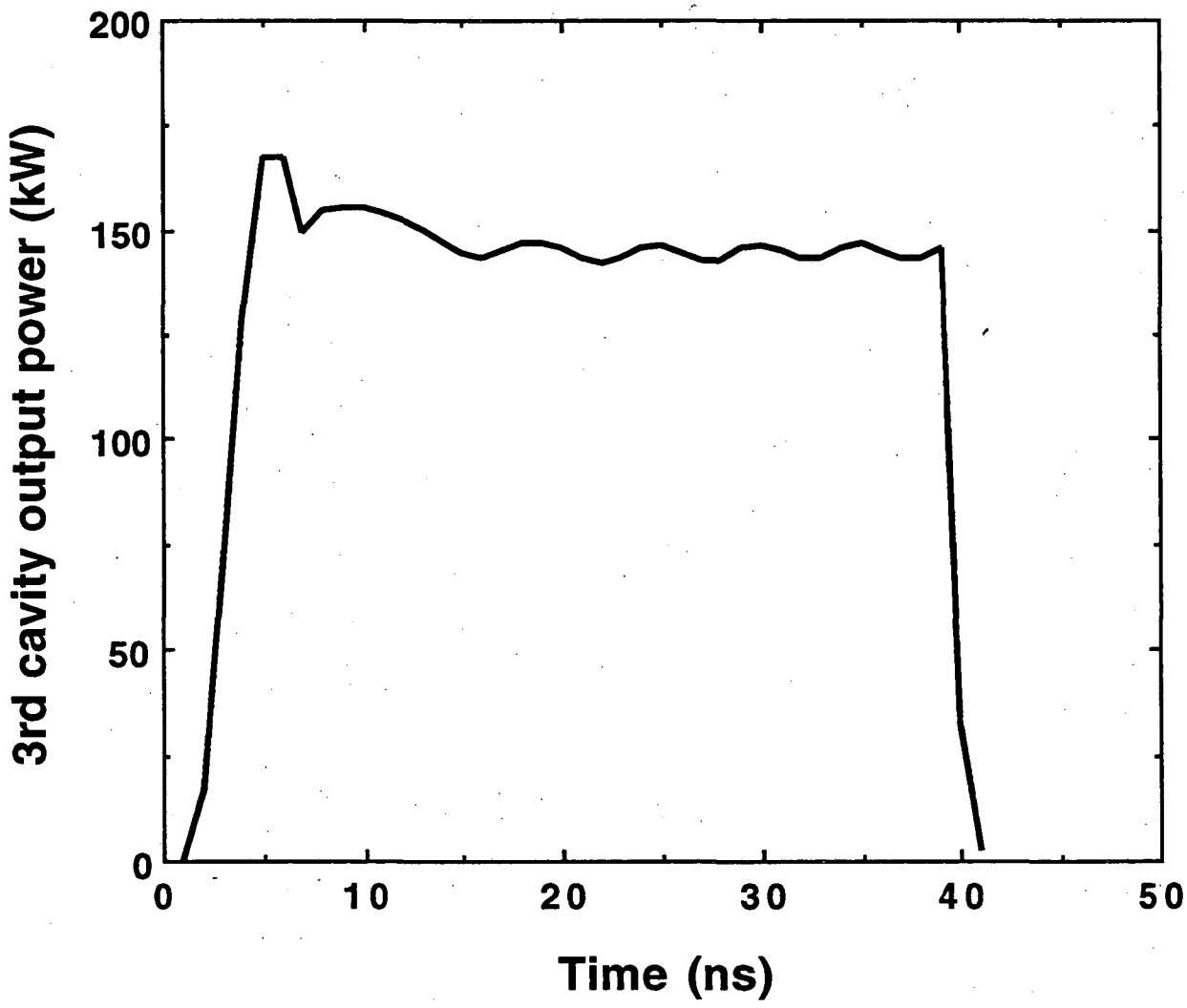
200
150
100
50
0
3rd cavity output power (kW)
0
10
20
30
40
50
Time (ns)

Fig.7

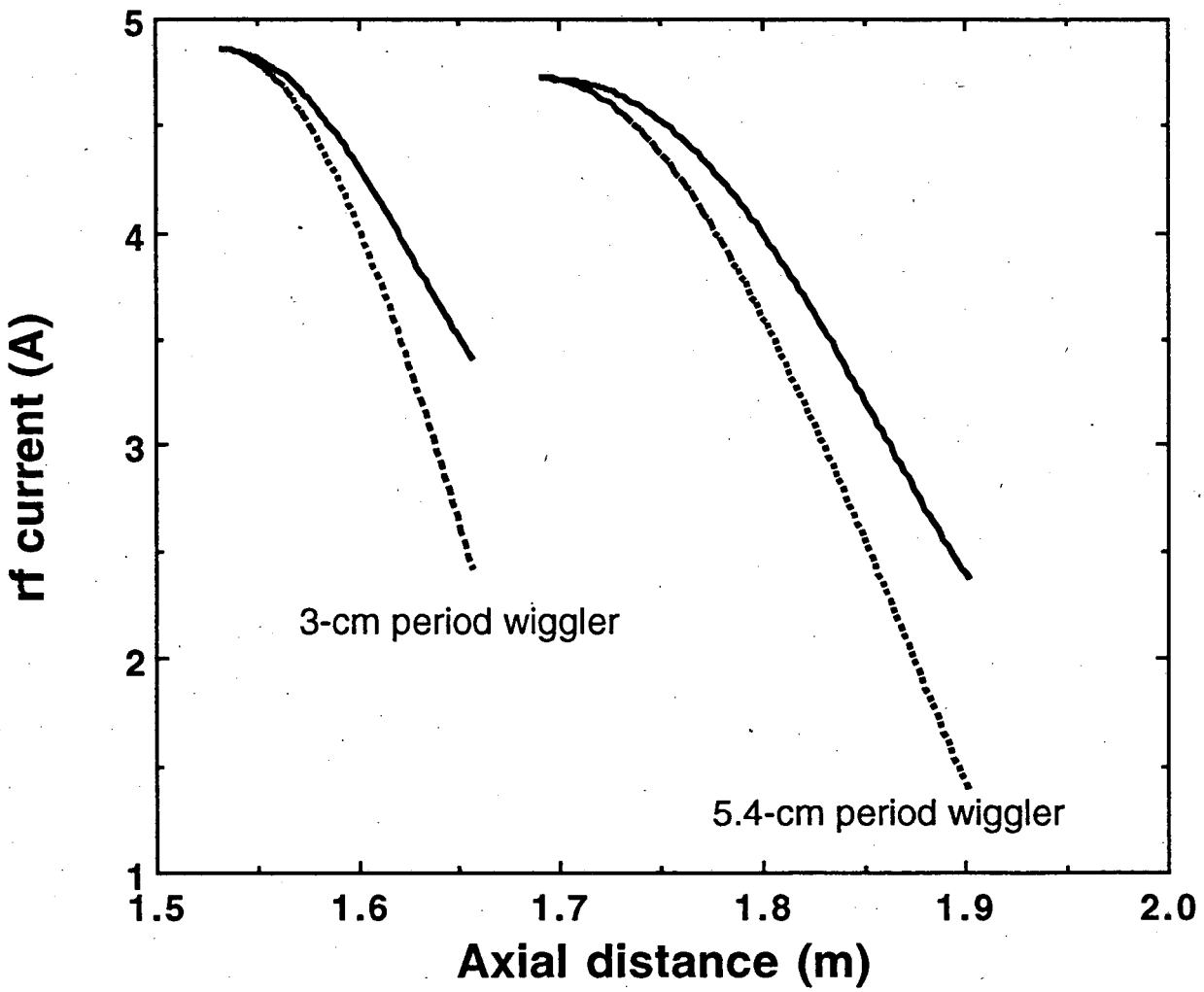
5
4
3
2
1
rf current (A)
1.5
1.6
1.7
1.8
1.9
2.0
Axial distance (m)
3-cm period wiggler
5.4-cm period wiggler

Fig.8

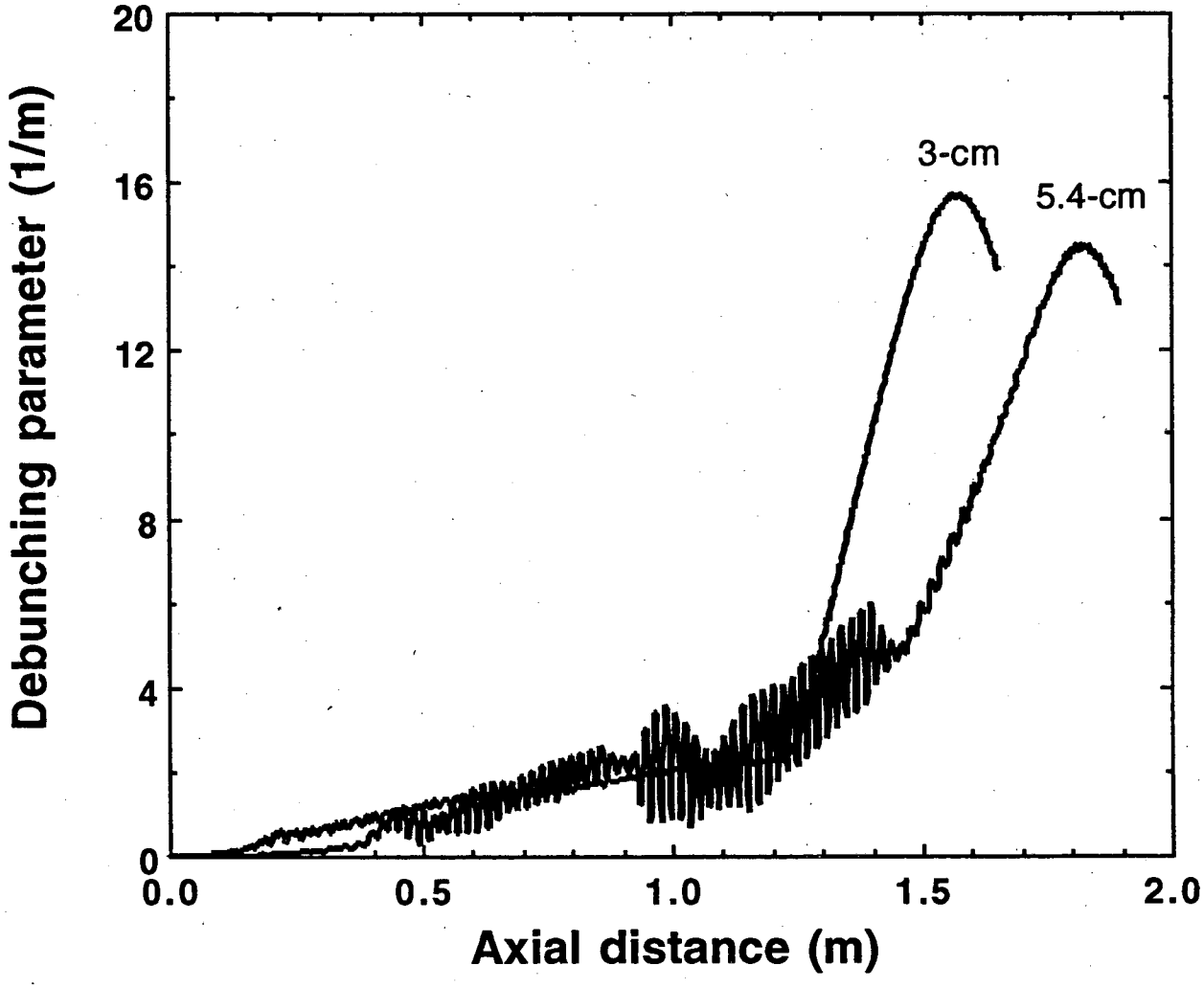
Debunching parameter (1/m)
20
16
12
8
4
0
0.0
0.5
1.0
1.5
2.0
Axial distance (m)
3-cm
5.4-cm

Fig. 9

LAWRENCE BERKELEY LABORATORY
UNIVERSITY OF CALIFORNIA
TECHNICAL INFORMATION DEPARTMENT
BERKELEY, CALIFORNIA 94720